Carbon 192 (2022) 61–70

Contents lists available at ScienceDirect

Carbon

journal homepage: www.elsevier.com/locate/carbon

# Extreme structure and spontaneous lift of spin degeneracy in doped perforated bilayer graphenes

Iu.A. Melchakova [a, b], T.G. Tenev [c], N.V. Vitanov [c], O.N. Tchaikovskaya [b], L.A. Chernozatonskii [d, e], B.I. Yakobson [f], P.V. Avramov [a, *]

[a] Department of Chemistry, Kyungpook National University, Daegu, South Korea
[b] Tomsk State University, 36 Lenin Ave, Tomsk, 634050, Russia
[c] Department of Physics, Sofia University, 5 James Bourchier Blvd, Sofia, 1164, Bulgaria
[d] Emanuel Institute of Biochemical Physics, Russian Academy of Sciences, 4 Kosigin st, Moscow, 119334, Russian Federation
[e] Research School Chemistry and Technology of Polymeric Materials, Plekhanov Russian University of Economics, Moscow, 117997, Russian Federation
[f] Rice University, Department of Materials Science and Nanoengineering, Department of Chemistry, and the Smalley Institute, Rice University, Houston, TX, 77005, United States

ARTICLE INFO

*Article history:*
Received 12 October 2021
Received in revised form
13 February 2022
Accepted 17 February 2022
Available online 21 February 2022

*Keywords:*
Nanoporous bigraphenes
Lift of spin degeneracy
Spin polarization
Doping
Non-relativistic spin-orbital interactions

ABSTRACT

Extreme structure and spin states of doped and undoped perforated bigraphenes was studied using DFT simulations. It was found that folded nanopores possess extremely high curvature of 0.34 $Å^{-1}$. Dramatic structural deformation causes severe changes of the chemical properties of carbon atoms localized at the nanopores converting the folded edges to local oxidative fragments. It was found that asymmetrical coordination of either Li, Ca, or Al to the nanopores is coupled with electron transfer from metal to edge carbon atoms and breakdown of local inversion symmetry. Li-, Ca-, and Al-doped perforated AA bigraphene revealed ferromagnetic spin ordering with magnetic moments of 0.38, 0.14, and 0.32$\mu_B$/unit cell, respectively, and spin polarization energy gain of 0.037eV for Ca-doped superlattice. It was shown that ferromagnetic spin ordering of bigraphene nanopores contradicts to the Nagaoka's theorem, which excludes strong electron correlations as a reason of spin polarization. Spontaneous lift of spin degeneracy was interpreted in terms of perturbing intense local electrostatic fields from extra electron charges localized at the nanopore edges, coupled with breakdown of space inversion and local translation invariances. It was shown that spin energy splitting is proportional to the matrix elements calculated on Bloch states with opposite wavevectors and perturbing electrostatic fields.



## 1. Introduction

Lift of spin-degeneracy in low-dimensional crystalline lattices and heterostructures is a fundamental challenge in condensed matter physics [1]. Recent finding of magnetism in atomically thin van der Waals low-dimensional materials and heterostructures [2,3] attracts an increasing interest in the investigation of magnetic phenomena at the nanoscale [4]. Standalone, real-space, interface-localized 2D electronic gas superlattice was experimentally observed [5] in a vertically stacked $Bi_2Se_3$/TMD (TMD = $MoS_2$, $MoSe_2$, $WS_2$, $MoSe_2$) 2D heterostructures. It was found that regular patterns of the electron gas are driven by interlayer potentials determined by Moiré atomic superlattices. A discovery of spin-photon interactions in heterostructures based on InAs quantum dots adjusted with GaNAs spin filter paves the way for remote spin encoding and writing of quantum memory as well as for remote spin control of spin−photon interfaces [6].

At the dawn of the study of magnetism at microscopic scale, Heisenberg [7] concluded that ferromagnetism could not exist in compounds consisting only of light elements. Nevertheless, later a soft ferromagnetism in charge-transfer salt (tetrakisdimethylaminoethylene)$C_{60}$ [(TDAE)$C_{60}$] was detected without remanence with atypical behavior of temperature dependence of the magnetization below Curie temperature Tc = 16.1 K ([8] and many other publications). The [(TDAE)$C_{60}$] lattice merohedral disorder gives rise to a distribution of π-electron exchange interactions between spins on neighboring $C_{60}$ molecules, originated due to charge transfer of N*p*-electrons from TDAE fragments, suggesting a microscopic origin for

* Corresponding author.
*E-mail address:* paul.veniaminovich@knu.ac.kr (P.V. Avramov).

https://doi.org/10.1016/j.carbon.2022.02.041
0008-6223/

the observed spinglass behavior of the magnetic state [9]. Ferromagnetism was also discovered in $C_{60}$ polymers like 2D rhombohedral $C_{60}$ polymer [10] which demonstrates typical ferromagnetism with saturation magnetization and large hysteresis. The temperature dependences of its saturation and remanent magnetization indicate a Curie temperature near 500 K. The ferromagnetism of all mentioned materials is realized based on the spin-ordering of regular *p*-derived carbon states.

A challenging 2D material based on superlattices of potential bumps (so-called quantum antidots) driven by folded holes in bilayer graphene (nanoporus bigraphene, NPBG) was theoretically predicted [11,12] and later obtained experimentally by either electron or ion bombardment [13–15] or by fabrication of large-area, sub-10 nm single- and bilayer graphene nanomeshes from block copolymer self-assembly [16]. Nanoporous bigraphene was studied using DFT technique by considering nanomesh lattices with different periodic arrangements [11]. It was found that the nanopores edge types cause specific bonding and hole shape formation, e.g. zig-zag edges form a closed structure with regular threefold coordination. The NPBG electronic properties are determined by the nanopores allowing one to fabricate materials with challenging band structures. Similar twisted NPBG with fused nanopores was recently proposed and theoretically studied as well [17]. It was found that proposed superlattices are stable and demonstrate various challenging electronic properties.

Bigraphene is a very promising material consisting of two graphene sheets stacked to each other either in AA or AB sequences [12]. Like in graphite, in-plane C–C bonding is realized via $\sigma$- and $\pi$-carbon-carbon bonds while weak van der Waals interactions of neighboring graphene sheets are responsible for out-of-plane bonding [18]. In particular, it was shown [18] that electronic structure of bigraphene is slightly different from the electronic structure of single layered graphene [19] and it can be considered as zero-gap semiconductor even having small band overlap (1.6 meV) [20].

A bigraphene piece of a precisely controlled alignment can be fabricated by “tear and stack” technique [21–24] by exfoliation of graphene flakes with consequent rotation and stacking on each other at arbitrary angles to achieve desirable mutual arrangement. Either electron or ion bombardment [13–15] can be used to create the holes in graphene fragments with consequent fusion of the hole edges to stabilize the lattice by saturation of the dangling bonds at opposite graphene flakes.

Nanoporous materials (NPM) and heterostructures based on NPMs with various atoms adsorbed at the pores are of great interest to design quantum materials, catalysts etc. [25,26]. Pristine and doped nanoporous bigraphene maybe a promising nanomaterial to lift spin degeneracy in 2D quantum materials due to extreme curvature of polarized pores and strong anisotropy of the potential perpendicular to its main plane. One can speculate that making nanopores in bilayer graphene is a promising way to gain extreme local electric fields at the nanoscale through record curvature of the nanopores.

In this study, a novel type of hybrid low-dimensional materials based on AA and AB nanoporous bigraphenes doped by light (Li, Ca, Al) *sp*-metals was theoretically proposed and studied using non-relativistic Density Functional Theory. It was found that fusion of the dangling bonds at the nanopore edges leads to formation of structural features of extremely high curvature up to 0.34 $Å^{-1}$ with unique electronegativity properties. Adsorption of *sp*-metal atoms leads to their oxidation by carbon lattice with charge transfer to strongly distorted carbon-carbon bonds of complex nature which form fused edges of the nanopores. The electronic structure calculations revealed spontaneous spin polarization of the carbon atoms at the nanopore edges of Li, Ca, and Al doped nanoporus bigraphene of AA morphology with 0.38, 0.14, and 0.32 $\mu_B$/unit cell, respectively with energy splitting between ferromagnetic and diamagnetic states for Ca-doped AA NPBG equal to 0.037 eV. Relativistic spin-orbital coupling and artificial spin contamination were ruled out as possible sources of spin-polarization by the composition of lattices with only light *sp*-elements and negligible spin-contamination errors. Using Nagaoka's theorem analysis, it was shown that electron correlation effects cannot be responsible for ferromagnetic spin ordering in doped nanoporous bigraphene lattices for either strong or weak repulsive potentials and all possible numbers of doping electrons. A new non-relativistic mechanism of lift of spin degeneracy by perturbing intense local electrostatic fields coupled with disruption of local space inversion and translation invariances was proposed based on symmetry analysis and perturbation theory. It was shown that combination of extra electronic charge with extremely high curvature of the nanopore edges generates Intense Local Electrostatic Fields (ILEF) inside the pores coupled with breakdown of local space inversion (SII) and translation invariances (TI) due to asymmetrical adsorption of metal ions. It was found that in terms of perturbation theory the spin splitting energy is proportional to the matrix elements of perturbed non-SII and non-TI electric field operator sandwiched by $s_u, k|$ and $|-k, s_u$ Bloch states.

The atomistic models of the lattices were developed to rule out the electronic correlation effects and the relativistic spin-orbital coupling from multi-level theoretical consideration. After Computation section, the results of DFT simulations of proposed pristine and doped NPBG lattices are presented coupled with an analysis of possible spin-contamination of spin-polarized electronic wave functions. Using the Nagaoka theorem analysis of the electronic structure of the AA NPBG pore core the strong electron correlations were ruled out as a reason of ferromagnetic spin polarization of *sp*-metal doped AA NPBG lattices. Symmetry analysis and perturbation approach were used to introduce the non-relativistic spin-orbital coupling terms and to interpret spin polarization of the lattices in terms of perturbing Intense Local Electrostatic Fields.

## 2. Computational details

All electronic structure calculations of low-dimensional crystalline lattices were performed using Vienna Ab-initio Simulation Package (VASP) [27–29] within Density Functional Theory (DFT) [30,31] and Periodic Boundary Conditions (PBC) framework. Plane wave basis set with projector augmented wave (PAW) method [32,33], GGA-PBE [34] functional and Grimme correction [35] for van-der-Waals interaction were used in the study. Mönkhorst-Pack Brillouin zone *k*-point sampling was implemented, and the *k*-point mesh contained $3 \times 3 \times 1$ *k*-points along *a*, *b* and *c* directions, respectively, was used for NPBG optimization. For DOS calculations $6 \times 6 \times 1$ *k*-point mesh was used. Non-collinear calculations were carried out using spin-orbital coupling (SOC) to determine electron spin orientation in metal-doped nanoporous bigraphene. A vacuum interval of 20 Å was set normal to the plane to avoid artificial interactions between adjacent unit cell images. In all calculations the cutoff energy was equal to 520 eV. During optimization procedure the maximum force acting on atoms less than 0.001 eV/Å was used as a stopping criterion for structural minimization. The atomic and electronic structure of $C_{36}H_{24}$ cluster was studied using *ab initio* B3LYP DFT potential [36–38] with 6–31G* basis set [39,40] to analyze the electronic structure of model AA nanoporous bigraphene core.

## 3. Results and discussion

### 3.1. Electronic structure of pristine and doped nanoporous bigraphene

The unit cell optimization for both 2D AA and AB bigraphene configurations was performed for perfect hexagonal cells ($a = b = 2.45$ Å, $c = 20.00$ Å) and then for bigraphene with double vacancies using $6 \times 6 \times 1$ supercells (Fig. 1 and S1). The pore etching was made by elimination of 6 carbon dimers with further structural optimization (Fig. 2). Energetic and structural characteristics of NPBGs are presented in Table 1. It was found that both AA and AB NPBGs are non-spin-polarized materials with slightly different cell parameters and very large energy difference (35.41eV) between the conformers caused by significant differences in the structure of the nanopores and resulting structural stress.

Both nanopores comprise 6 eight-member rings which share common carbon-carbon bonds either all parallel (AA type) or inclined (AB type) to the main nanopore axis (Fig. 2). The AA and AB nanopore cores are highly symmetrical and belong to either $D_{6h}$ or $D_{3d}$ symmetry groups, respectively. The AA and AB nanopore internal curvatures were estimated by the best fitting of both cross sections (8 points each) by forth order polynomial and it was found that they are equal to 0.336 $Å^{-1}$ and 0.070 $Å^{-1}$, respectively.

The mutual graphene layer orientation has a crucial impact on electronic properties of NPBG, i.e. NPBG(AA) possess semiconducting properties with 0.65 eV band gap while NPBG(AB) is a metal (Fig. 3). The pores drastically change the bigraphene DOS completely eliminating electronic density at the Fermi level which is attributed to the Dirac cones of pristine graphene and bigraphene and converting perfect bigraphene from semimetallic either to narrow band gap semiconducting NPBG(AA) or metallic NPBG(AB).

To enhance the polarization effects of NPBG nanopores by extra charges and to ruled out the relativistic spin-orbital coupling which is important for *d*- and *f*-elements, the pores were doped by either Li (Fig. 4a), Ca (Fig. 4b), or Al (Fig. S2) atoms which provide additional 1, 2, or 3 electrons of *s*- ($^2S_{\frac{1}{2}}$ Li, $^1S_0$ Ca) or *s*- and *p*-nature ($^2P_{\frac{1}{2}}$ Al), respectively, to strongly distorted carbon-carbon bonds at the

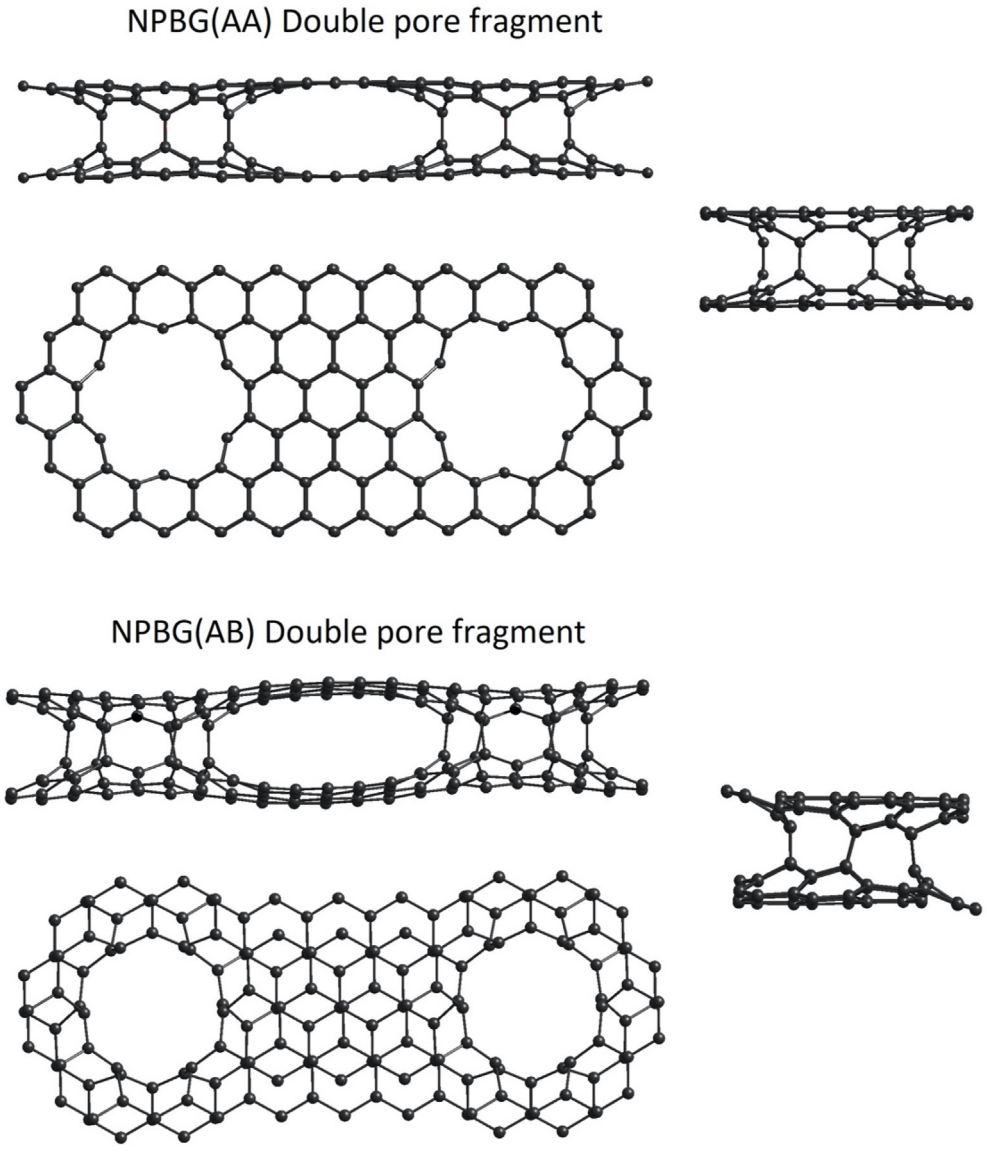


**Fig. 1.** Top: Three projections of a fragment of 2D AA nanoporus bigraphene with two pores. Two $D_{6h}$ pores are connected through ellipse-shaped channel. Bottom: Three projections of a fragment of 2D AB nanoporus bigraphene with two $D_{3d}$ pores connected through ellipse-shaped channel.

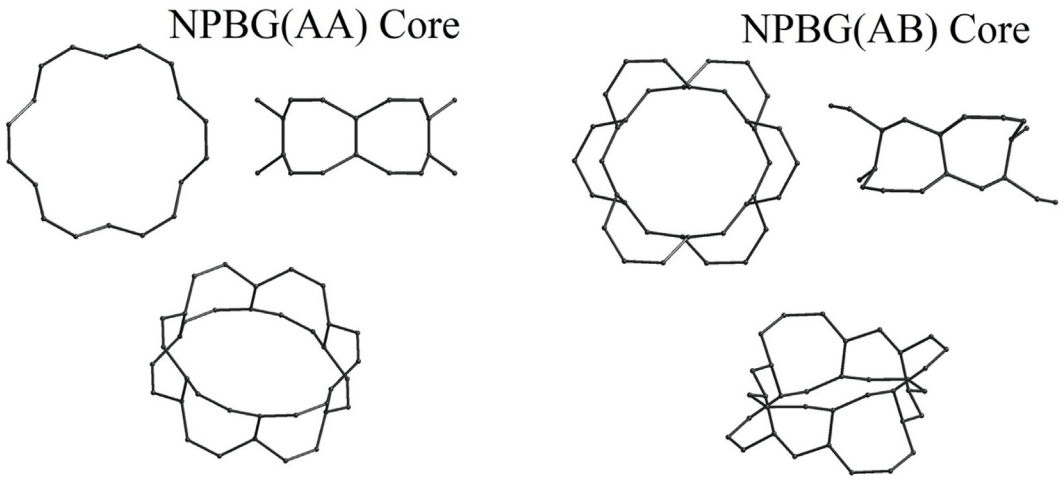


**Fig. 2.** Left: Three projections of detailed atomic structure of the central core of a pore in AA-stacked bigraphene. The core of AA pore of $D_{6h}$ symmetry consists of 6 equivalent buckled octagonal carbon rings, fused by common carbon-carbon bonds, parallel to the main axis of the nanopore. Right: Three projections of atomic structure of the central core of a pore in AB-stacked bigraphene. The pore of $D_{3d}$ symmetry consists of 6 equivalent deformed octagonal carbon rings, fused by common carbon-carbon bonds with opposite fragments mutually oriented in opposite directions. Fused C–C bonds are inclined in respect to the main axis of AB pore.

**Table 1**
The energy difference ΔE (eV), the structural parameters (Å), band gap values (eV), and edge curvatures ($Å^{-1}$) of AA and AB NPBGs.

| Type | ΔE, eV | a, Å | Band gap, eV | Edge curvature, $Å^{-1}$ |
|---|---|---|---|---|
| AA | 35.41 | 14.74 | 0.53 | 0.336 |
| AB | 0.00 | 14.75 | metal | 0.070 |

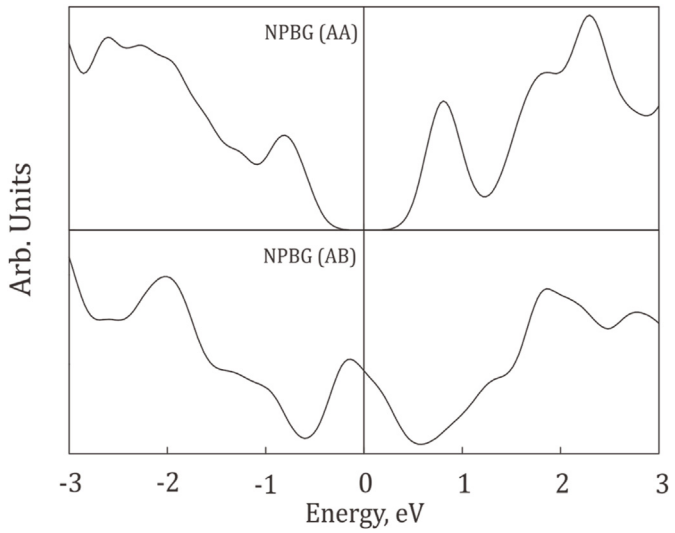


**Fig. 3.** Total density of states of NPBG in AA (top) and AB (bottom) stacking sequences.

nanopore edges. It is worth to note that for light elements like Li, C, Ca, and Al, spin is a good quantum number because of negligibly small corresponding spin-orbital coupling constants. The polarization effects in hybrid Me@NPBG (M = Li, Ca, Al) lattices can be enhanced by opposing the extra electronic charges by $Li^+$, $Ca^{2+}$, or $Al^{3+}$ counterions as well as combined with possible elimination of local symmetry caused by asymmetrical coordination of metal ions.

Structural parameters, magnetic moments and band gap values of all Me@NPBGs calculated at PBC PAW PBE level of theory are presented in Table 2. Because of relatively small deviation of $Li^+$ and $Al^{+3}$ positions from the AA pore centers, the C–Me bond length were averaged as arithmetic mean among the interatomic distances inside the pores. Electronic structure calculations revealed asymmetrical positions of $Li^+$, $Ca^{2+}$, or $Al^{3+}$ ions inside the NPBG(AA) pores, which effectively eliminate local symmetry of doped nanopores.

In Me@NPBG(AA) $Li^+$ and $Al^{+3}$ ions are localized rather close to the center of the pores with average Li–C and Al–C distances equal to 3.252 and 3.263 Å, respectively (Table 2), which is much longer than corresponding bond length in $Li_2C_2$ (2.212 and 2.402 Å [41] and $Al_4C_3$ (1.898, 1.944, 2.170, and 2.223 Å [42]) carbides. In contrast to $Li^+$ and $Al^{+3}$, the $Ca^{+2}$ (Fig. 4b) occupies very asymmetric position with shortest/longest Ca–C bonds equal to 2.583/3.797 Å, both of each much longer the Ca–C bond in $CaC_2$ of 2.421 Å [43].

In contrast to AA conformers, $Li^+$ and $Al^{+3}$ ions inside the pores of Me@NPBG(AB) are localized very asymmetrically with much closer positions to one of external nanopore edge. In fact, both ions are coordinated not to 12 (AA case), but rather to two carbon atoms to the same ($Li^+$) or opposite ($Al^{+3}$) nanopore edges. $Ca^{2+}$ ion in NPBG(AB), reveals almost symmetrical coordination rather close to the center the pore with shortest/longest Ca–C bonds equal to 2.825/3.217 Å.

Doping of both NPBG(AA) and NPBG(AB) by either Li, Ca, or Al causes electronic transfer of one, two or three extra electrons from metal 2*s* (Li), 3*s* (Ca, Al) and 3*s*, 3*p* (Al) orbitals to 6 (in case of Li and Al) or just 1 (Ca@NPBG(AA)) π-states localized at C–C bonds which form the inner core of the nanopores (Fig. 5 and S2), making the pores strongly electrically polarized. It is necessary to note that artificial small delocalized charge transfer to the edges of bigraphene unit cell is caused by slight misalignment (0.02 Å, Table 2) of Ca@NPBG(AA) and NPBG(AA) lattices used to calculate charge transfer distribution.

The induced magnetic moments per unit cells (0.38, 0.14, and 0.32 $\mu_B$ for Li@NPBG(AA), Ca@NPBG(AA) and Al@NPBG(AA), respectively (Table 2), demonstrate the direct impact of structure and symmetry of the pores on the spin states of the Me@NPBGs. In particular, either highly symmetrical $D_{6h}$ or $D_{3d}$ AA and AB undoped conformers do not reveal any magnetic moments. Distorted atomic structure and extremely high curvature of both types of nanopores leads to oxidation of metal atoms with electron transfer to 6 (Li@NPBG(AA) and Al@NPBG(AA) or 1 (Ca@NPBG(AA) C–C bonds,

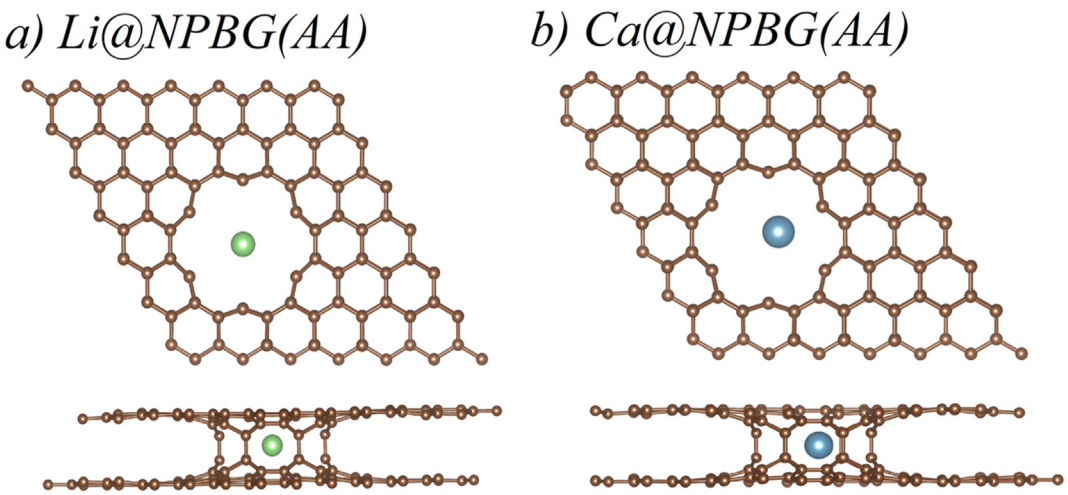


**Fig. 4.** a) Top and side views of Li@NPBG in AA stacking sequence. b) Top and side views of Ca@NPBG in AA stacking sequence. Carbon atoms are denoted in brown, $Li^{+}$, and $Ca^{+2}$ ions are denoted in green, and blue. (A colour version of this figure can be viewed online.)

**Table 2**
C–Me bond lengths (Å), magnetic moments ($\mu_B$) per unit cell, unit cell parameters (Å), and curvature of the nanopore edges ($Å^{-1}$) of Me@NPBG heterostructures. In the case of AA conformers averaged values are presented. In the case of AB-heterostructures the C–Me bond length for carbon atoms which belong to different carbon layers are separated by slash.

| Ion | Type | C–Me bond length, Å | Magnetic moment, $\mu_B$ | Unit cell parameter *a*, Å | Curvature $Å^{-1}$ |
|---|---|---|---|---|---|
| Li | AA | 3.252 | 0.38 | 14.74 | 0.336 |
| | AB | 2.417, 2.438–3.010/2.985–3.422 | 0.00 | 14.75 | 0.070 |
| Ca | AA | 2.583/3.797 | 0.14 | 14.72 | 0.336 |
| | AB | 2.825/3.217 | 0.00 | 14.72 | 0.070 |
| Al | AA | 3.263 | 0.32 | 14.73 | 0.336 |
| | AB | 2.108–3.583/2.195–3.64 | 0.00 | 14.73 | 0.070 |

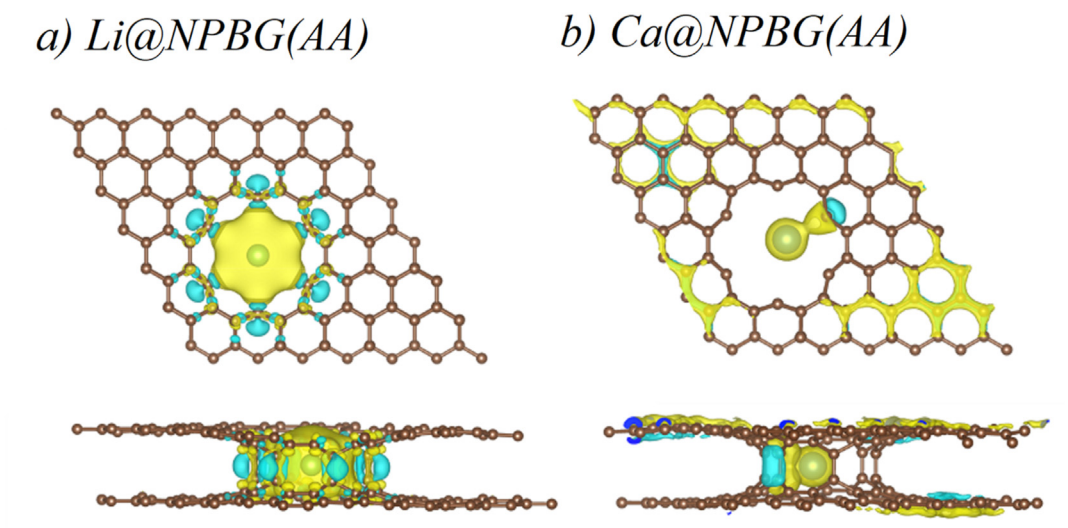


**Fig. 5.** Charge transfer from Li, and Ca to carbon core of NPBG(AA). Negative charge transfer is depicted in cyan, positive charge transfer is depicted in yellow. Artificial small delocalized charge transfer to the edges of bigraphene unit cell in case of Ca@NPBG(AA) is caused by slight misalignment of Ca@NPBG(AA) and NPBG(AA) lattices. (A colour version of this figure can be viewed online.)

which form the inner pore structures (Fig. 2). Generated intense local electrostatic field at the nanopore is induced by extreme curvature of 0.336 $Å^{-1}$ of the pores combined with extra electronic charge and opposed $Li^{+}$, $Ca^{2+}$, or $Al^{3+}$ counterions.

Small curvature radii ($R_{AA}$ = 2.98 Å and $R_{AB}$ = 14.29 Å) of both folded NPBG nanopores is a source of extreme local electric fields:

$$V = ze/R \quad (1)$$

where *ze* is electronic charge, localized at nanopore folded edges and *R* is curvature radius, which promotes enhanced chemi- and physisorption [13,14]. The curvature of $sp^2$ lattice leads to enhanced electronegativity of the carbon atoms and oxidation of dopant

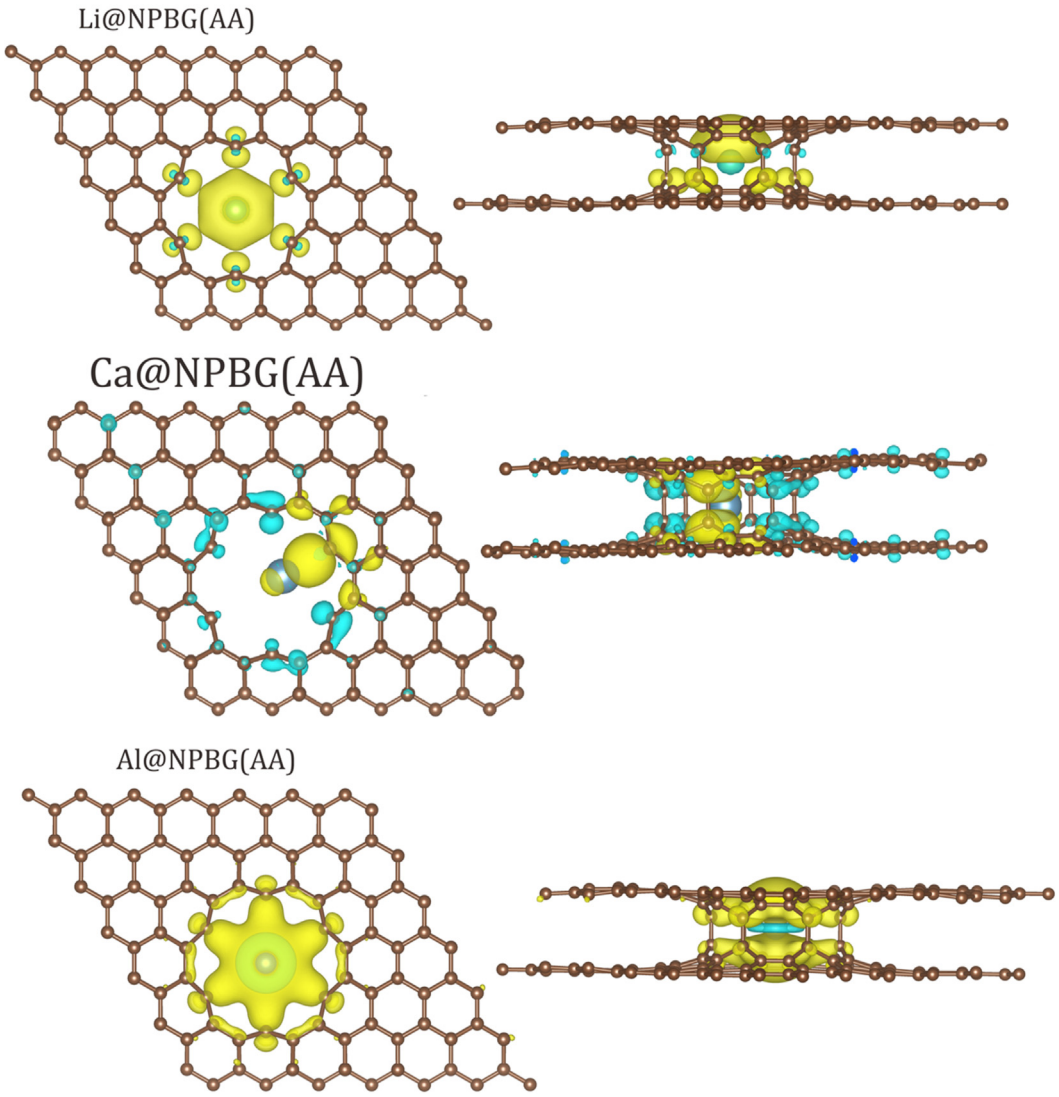


**Fig. 6.** Spatial spin density distribution (top and side views) of Li@NPBG(AA) (top); Ca@NPBG(AA) (in the middle); and Al@NPBG(AA) (bottom). Spin-up density is depicted in yellow, and spin-down one is depicted in cyan. Carbon atoms are denoted in brown. (A colour version of this figure can be viewed online.)

metal atoms [44]. Positive and negative charges localized at the nanopores combined with extreme local curvature is a source of intense local electrostatic fields. Combination of ILEF with broken inversion and translation invariances [45] may generate spin energy splitting up to 0.1 eV for light elements like Ne atom [46–48].

To estimate the energy splitting between ferromagnetic and diamagnetic states and to exclude the influence of odd number of electrons per unit cell, the total energies of FM spin-ordered and diamagnetic unpolarized states of Ca@NPBG(AA) were calculated. It was found that Ca@NPBG(AA) diamagnetic state is higher in energy the FM one by 0.037 eV.

Following approximate spin projection (AP) scheme [49–52] the spin contamination error (SCE) is proportional to the energy difference between high- and low-spin states (see, for example [51]). The AP approach was successfully implemented in VASP [27–29] and used for unrestricted PW DFT PBC geometry optimization of correlated crystals like NiO and MnO [52] for which it was found that SCE corrections should be taken into account during structural optimization. In contrast to heavy elements like Mn and Ni, SCEs for the systems composed only by the light elements were found to be negligible [52]. For example, for $H_2$ dimer the SCE [52] was found to be 0.027 eV, which is very close to SCE for Ca@NPBG(AA) (0.037 eV). It is necessary to note that both Li and Al are light atoms which have doublet ground state for which the SCE is equal to 0 by definition since the high- and low-spin states are just equivalent to each other. Summarizing, for all considered Me@NPBG(AA) heterostructures the spin contamination of ferromagnetically ordered states is negligibly small and can be ruled out as a source of artificial spin polarization.

It is clearly seen (Fig. 6) that all Me@NPBG(AA) demonstrate significant spatial lift of spin degeneracy, i.e. the electrons with spin-up (yellow color) are localized differently in comparison with spin-down ones (in cyan). The direction of spin alignment was calculated using SOC and it was found to be parallel to *z*-direction. The Me@NPBG(AB) reveal no magnetic moments which excludes the spin polarization of 2D materials which can be attributed to much smaller AB nanopore curvature equal to 0.070 $Å^{-1}$ (Table 2).

Densities of states calculated for Me@NPBG(AA) demonstrate dramatic impact of Me electronic states on TDOS at the Fermi level, effectively converting semiconducting NPBG(AA) to metallic state (Fig. 7) by 0.4 eV energy shift. Partial density of states of Li, Ca and Al ions at the vicinity of the Fermi level is almost equal to 0, which

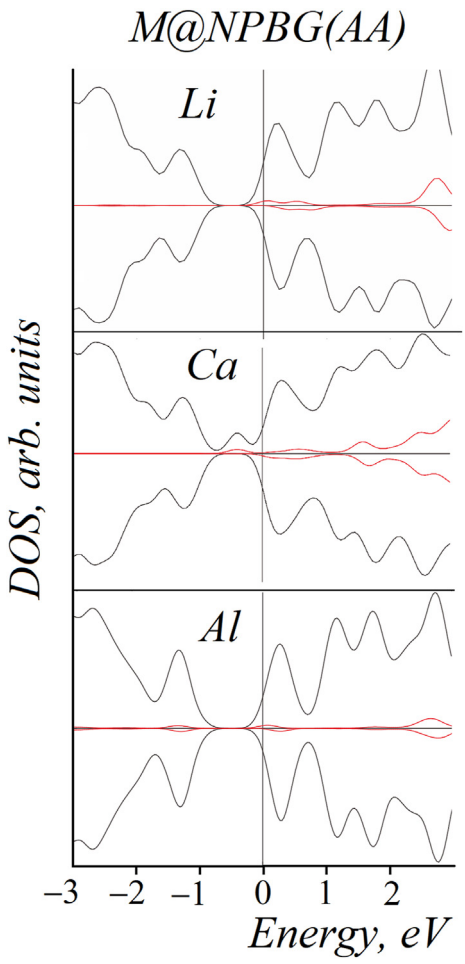


**Fig. 7.** The densities of states of Li@NPBG(AA) (top), Ca@NPBG(AA) (middle), and Al@NPBG(AA) (bottom). Total densities (TDOS) are depicted in black, and partial densities of Li, Ca, Al (PDOS) are depicted in red. Spin-up DOSes are depicted with positive sign, spin-down DOSes are depicted with negative sign. (A colour version of this figure can be viewed online.)

directly indicate perfect +1, +2, and +3 oxidative states of the ions.

The electronic properties of Me@NPBG(AB) remain the same as for NPBG(AB) and the impact of *sp*-metal doping is not observed, possessing metallic properties with absence of spin-polarization. For all cases Li, Ca, or Al PDOS intensities in the vicinity of Fermi level are close to zero with minor impact on TDOS shape (Fig. S3).

The most reasonable way to synthesize NPBG is ion bombardment followed by treatment of the samples under high pressure, which should lead to formation of irregular fused nanopores. Consequent metal doping of the nanoporous bigraphene should lift spin degeneracy with formation of irregular paramagnetic 2D material rather than ferromagnetic lattice of spin centers due to the stochastic nature of nanopores fabricated by ion treatment.

### 3.2. Spin ordering and Nagaoka's theorem

Let's consider Nagaoka's theorem [53] to take into account the effect of strong electron correlations on the spin states of hexagonal NPBG(AA) (Figs. 1, 2, S1) and Me@NPBG(AA)s (Fig. 4) lattices. Symmetry analysis and *ab initio* B3LYP/6-31G* calculations of $D_{6h}$ symmetry $C_{36}H_{24}$ cluster (Fig. 8), which represents the core structure of NPBG(AA), revealed $B_{1g}$ LUMO and $E_{2u}$ LUMO+1 states, with LUMO − LUMO+1 gap $E_b$ = 0.92 eV. In total, both two-fold degenerate $B_{1g}$ and four-fold degenerate $E_{2u}$ states provide 6 vacancies to accept doping electrons from metal atoms. To consider half-filled band Nagaoka's model, the NPBG(AA) nanopore is equivalent to 3 vacant double-degenerate states to accept doping electrons. Since pristine NPBG(AA) pore core has no additional electrons, its ground state can be considered as a vacuum state without any correlation effects which may cause spin polarization of the lattice.

According to Nagaoka's theorem, for the case of sufficiently strong repulsive potential *U*, *hcp* lattice, and $N_e > N$, where $N_e$ is a number of electrons and *N* is the number of states to be filled by 2 *N* electrons, the maximum spin state is the ground state of the system, and it is not the ground state for $N_e \leq N$. For the case of NPBG(AA) with $N = 3$ and $N_e = 1, 2$, and 3 for Li-, Ca-, and Al-doped NPBG(AA)s, the ferromagnetically-ordered state cannot be the ground state of either Li@NPBG(AA), Ca@NPBG(AA), or

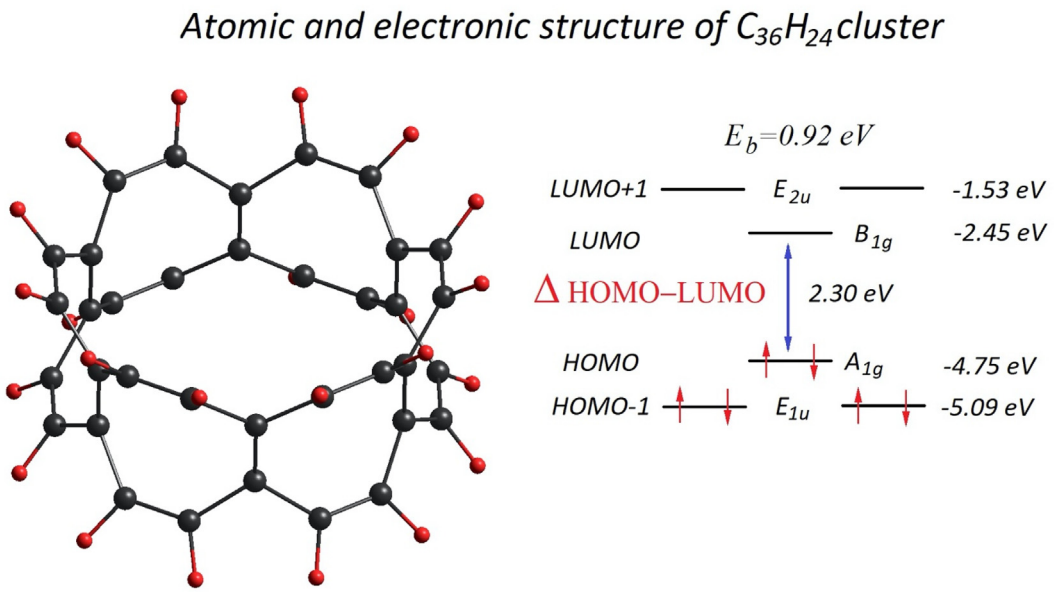


**Fig. 8.** Atomic and electronic structure of $C_{36}H_{24}$ cluster of $D_{6h}$ symmetry. Carbon atoms are presented in black and hydrogen atoms are presented in red. Spin up/spin down electrons are presented by up/down arrows. At B3LYP/6-31G* level of theory the LUMO $B_{1g}$ − LUMO+1 $E_{2u}$ gap $E_b$ = 0.92 eV. The HOMO-LUMO gap ΔHOMO-LUMO = 2.30 eV. (A colour version of this figure can be viewed online.)

Al@NPBG(AA) lattices.

Let's consider the case with $N_e > N$. The trivial case of $N_e = 6$ is equivalent to vacuum state, so it must be diamagnetic. Let's estimate repulsive potential $U$ for $N_e = 4$, and 5. According to Nagaoka's theorem, for *hcp* lattice, and $U < E_b \times N/|N - N_e|$, where $E_b$ is the bandwidth, the ferromagnetically ordered spin state is not the ground state of the system. So, for $E_b = 0.92$ eV and $N_e = 4$ $U = 2.8$ eV, and for $N_e = 5$ $U = 1.4$. eV. Both values are of the same order of magnitude the $U$ values for the first transition metal atoms V (3.1 eV), Co (3.3 eV), and Cr (3.5 eV) [54]. It is worth to note that $U$ values for light *sp*-elements (H, Li, C, Ca, Al) are equal to 0. So, according to Nagaoka's theorem, for either sufficiently strong or weak ($U$ < 1.4 eV) repulsive potentials, for all possible occupation numbers $N_e = 1$–5 electrons, the FM state is not a ground state for doped *hcp* NPBG(AA) lattice, which unequivocally excludes correlation effects as the main reason of spin polarization of *sp*-metal doped nanoporous bigraphene.

### 3.3. Symmetry analysis and perturbation theory consideration

Let's consider a low-dimensional crystalline lattice which lacks the SII conditions. Taking into account the spin degree of freedom, the non-perturbed *non*-SII *non*-relativistic Hamiltonian for the lattice can be written

$$\widehat{H} = \frac{\widehat{p}^2}{2m}\widehat{\sigma}_0 + V_0(r)\widehat{\sigma}_0 - e\varphi(r)\widehat{\sigma}_0 \tag{2}$$

where $V_0(r) = -e\varphi_0(r)$ is SII potential energy of a *non*-relativistic electron with two quantum numbers, the crystal wavevector $k$ and the spin index $s_u$, which is the eigenvalue of $u$-component of spin operator $\widehat{S}$, and $\widehat{\sigma}_0$ is 2 × 2 identity matrix. The term $\varphi(r)$ is antisymmetric $\widehat{I}\varphi(r)\widehat{I}^{+} = -\varphi(r)$ with respect to inversion symmetry operation and anti-commutes with inversion operator $\widehat{I}$, which effectively lifts the spin degeneracy

$$E_{k,s_u} \neq E_{k,-s_u} \tag{3}$$

Let's consider the spin-rotation operator $\widehat{R}^{s}_{u}(\varphi) = e^{-i\varphi\widehat{S}_u}$ for arbitrary axis $u$ which commutes with the Hamiltonian for arbitrary $\varphi$: $[\widehat{H}, \widehat{R}^{s}_{u}] = 0$ keeping SU(2) invariance. For unperturbed Hamiltonian the states $|k, s_u>, |k, -s_u>, |-k, s_u>, |-k, -s_u>$ span a 4 four-fold degenerate subspace $\varepsilon^0_k$ for the energy $E_{k,s_u} = E_{-k,-s_u} = E_{-k,s_u} = E_{k,-s_u}$, which directly contradicts with the relation (3) $E_{k,s_u} \neq E_{k,-s_u}$.

To avoid the paradox, let's consider a small perturbation $\delta V$, which consists of *non*-SII electrostatic potential $\varphi(r)$ with anticommutator $\{\varphi(r), \widehat{I}\} = 0$ and introduce two spin-orbit coupling terms: $\widehat{U}_1 = \frac{\hbar}{4m^2c^2}\widehat{\sigma}\cdot(\nabla V_0(r)\times\widehat{p})$ and $\widehat{U}_2 = -\frac{e\hbar}{4m^2c^2}\widehat{\sigma}\cdot(\nabla\varphi(r)\times\widehat{p})$.

With the spin-orbital coupling, the small perturbation can be written as

$$\delta V = -e\varphi(r) + \widehat{U}_1 + \widehat{U}_2 \tag{4}$$

The first-order energy correction $E^{(1)}_k$ can be found from the secular equation $\left[\widehat{P}^0_k\delta V\widehat{P}^0_k\middle|0_k> - E^{(1)}_k\right] = 0$ where $\widehat{P}^0_k$ is the projector to the subspace $\varepsilon^0_k$.

The *non*-SII perturbing electrostatic field $\varphi'(r)$ with corresponding energy $V'(r) = -e\varphi'(r)$ does not satisfy both TI and SII conditions: $\widehat{T}_{R_n}V'(r)\widehat{T}^{+}_{R_n} \neq V'(r)$; $\widehat{I}V'(r)\widehat{I}^{+} \neq V'(r)$. Let's apply Bloch theorem to the matrix element

$$\left\langle s_u, k|V'(r)|-k, s_u\right\rangle \neq e^{2ikR}\left\langle s_u, k\middle|V'(r)\middle|-k, s_u\right\rangle \tag{5}$$

and introduce the notation $\beta' = \langle k|V'(r)|-k\rangle = \langle s_u,k|V'(r)|-k,s_u\rangle$. Since the electrostatic field does not contain an operator acting directly on spin degree of freedom, the $s_u$ component maybe skipped in the expression. For any given $k$ and arbitrary translation vector $R$ one can write: $\beta' \neq e^{2ikR}\beta'$, therefore $\beta' \neq 0$. Then, the first-order energy correction can be determined as $E^{(1)\pm}_k = a_1 \pm \Delta E^{(1)}_k/2$ with the spin splitting energy

$$\Delta E^{(1)}_k = 2\sqrt{a_2^2 + |c_2|^2 + |\beta'|^2} \tag{6}$$

For the simplest case of SII system the splitting energy $\Delta E^{(1)}_k = 2|\beta'|$ has contributions only from electrostatic field, since $a_2$ and $c_2$ matrix elements are equal to 0, where $a_1 = \langle s_u, k|\widehat{U}_1|k, s_u\rangle$, $a_2 = \langle s_u, k|\widehat{U}_2|k, s_u\rangle$, $c_2 = \langle s_u, k|\widehat{U}_2|k, -s_u\rangle$.

A detailed derivation of spin energy splitting can be found in Supplementary Material (SM) Section.

## 4. Conclusion

Novel promising class of 2D nanoporous spin-polarized materials constituted only by light *sp*-elements (Li, C, Ca, Al) with visible lift of spin degeneracy was theorized using GGA PW PBC electronic structure calculations. It was shown that stacking sequence of graphene fragments determines the atomic structure and properties of NPBGs. Folded nanometer size pores in bilayer graphene generate intense local electrostatic perturbing fields caused by extra electron charges localized at the folded edges of extreme curvature up to 0.34 $Å^{-1}$. It was found that Li-, Ca-, and Al-doped NPBG(AA) lattices have ferromagnetic ground states with 0.38, 0.14, and 0.32 $\mu_B$/unit cell with spin density localized at carbon atoms which form the pore edges. It was shown that spin contamination is negligible for all Me@NPBG(AA) heterostructures and can be ruled out as an artificial source of spin polarization. For the case of even number of doping electrons ($N_e = 2$, Ca@NPBG(AA)) the relative energy of diamagnetic state is equal to 0.037 eV in respect to ferromagnetic ground state. Based on Nagaoka's theorem analysis, strong electron correlations were excluded as the main course of the lift of spin degeneracy in NPBG hexagonal lattices for all degrees of doping. For proposed heterostructures, relativistic spin-orbital coupling is ruled out as well since the lattices consist only of light elements, for which spin is a good quantum number and all relativistic effects are negligible. Novel mechanism of lift of spin degeneracy by perturbing local intense electrostatic fields in low-dimensional lattices with broken local inversion and translation symmetries was proposed. Using symmetry analysis and perturbation theory, it was found that the energy splitting between the spin channels is proportional to the matrix elements calculated on Bloch states with opposite wavevectors and perturbing electrostatic field with broken inversion and translation invariances. Stochastic lattices of doped irregular nanopores in AA bigraphene formed by ion bombardment with consequent high-pressure treatment and metal doping is expected to reveal 2D paramagnetic properties rather than ferromagnetic regular lattice of spin.

## CRediT authorship contribution statement

**IuA. Melchakova:** DFT calculations, graphics, discussions of the results, Writing –- original draft. **T.G. Tenev:** Symmetry analysis and perturbation theory consideration of lift of spin degeneracy by

extreme electric fields. Discussions of the results and manuscript preparation. **N.V. Vitanov:** Symmetry analysis and perturbation theory consideration of lift of spin degeneracy by extreme electric fields. Discussions of the results and manuscript preparation. **O.N. Tchaikovskaya:** Discussions of the results and manuscript preparation. **L.A. Chernozatonskii:** Initial atomistic models, of NPBG, discussions of the results and manuscript preparation. **B.I. Yakobson:** Discussions of the results and manuscript preparation. **P.V. Avramov:** Supervision, of the study, Nagaoka analysis, discussions of the results and manuscript preparation.

## Declaration of competing interest

The authors declare that they have no known competing financial interests or personal relationships that could have appeared to influence the work reported in this paper.

## Acknowledgments

This work was supported by Russian Science Foundation (Project 19-73-10015).

## Appendix A. Supplementary data

Supplementary data to this article can be found online at https://doi.org/10.1016/j.carbon.2022.02.041.

## References

[1] Yu A. Bychkov, E.I. Rashba, Properties of a 2D electron gas with lifted spectral degeneracy, JETP Lett. (Engl. Transl.) 39 (1984) 78–81. http://www.jetpletters.ac.ru/ps/1264/article_19121.shtml.
[2] B. Huang, G. Clark, E. Navarro-Moratalla, D.R. Klein, R. Cheng, K.L. Seyler, D. Zhong, E. Schmidgall, M.A. McGuire, D.H. Cobden, W. Yao, D. Xiao, P. Jarillo-Herrero, X. Xu, Layer-dependent ferromagnetism in a van der Waals crystal down to the monolayer limit, Nat 546 (2017) 270–273, https://doi.org/10.1038/nature22391, 2017 5467657.
[3] C. Gong, L. Li, Z. Li, H. Ji, A. Stern, Y. Xia, T. Cao, W. Bao, C. Wang, Y. Wang, Z.Q. Qiu, R.J. Cava, S.G. Louie, J. Xia, X. Zhang, Discovery of intrinsic ferromagnetism in two-dimensional van der Waals crystals, Nature 546 (2017) 265–269, https://doi.org/10.1038/nature22060.
[4] Z. Guguchia, A. Kerelsky, D. Edelberg, S. Banerjee, F. Von Rohr, D. Scullion, M. Augustin, M. Scully, D.A. Rhodes, Z. Shermadini, H. Luetkens, A. Shengelaya, C. Baines, E. Morenzoni, A. Amato, J.C. Hone, R. Khasanov, S.J.L. Billinge, E. Santos, A.N. Pasupathy, Y.J. Uemura, Magnetism in semiconducting molybdenum dichalcogenides, Sci. Adv. 4 (2018) eaat3672, https://doi.org/10.1126/sciadv.aat3672.
[5] Z. Hennighausen, C. Lane, I.G. Buda, V.K. Mathur, A. Bansil, S. Kar, Evidence of a purely electronic two-dimensional lattice at the interface of TMD/Bi 2 Se 3 heterostructures, Nanoscale 11 (2019) 15929–15938, https://doi.org/10.1039/c9nr04412d.
[6] Y. Huang, V. Polojärvi, S. Hiura, P. Höjer, A. Aho, R. Isoaho, T. Hakkarainen, M. Guina, S. Sato, J. Takayama, A. Murayama, I.A. Buyanova, W.M. Chen, Room-temperature electron spin polarization exceeding 90% in an opto-spintronic semiconductor nanostructure via remote spin filtering, Nat. Photonics (2021), https://doi.org/10.1038/s41566-021-00786-y.
[7] W. von Heisenberg, Zur Theorie des Ferromagnetismus, Zeitschrift für Physic 49 (1928) 619–636.
[8] P.-M. Allemand, K.C. Khemant, A. Koch, F. Wudl, K. Holczer, S. Donovan, G. Gruner, J.D. Thompson, Organic molecular soft ferromagnetism in a fullerene C60, Science 253 (1991) 301–302, https://doi.org/10.1126/science.253.5017.301.
[9] D. Mihailovic, D. Arcon, P. Venturini, R. Blinc, A. Omerzu, P. Cevc, Orientational and magnetic ordering of buckyballs in TDAE-C60, Science 268 (1995) 400–402. https://www.science.org/doi/10.1126/science.268.5209.400.
[10] T.L. Makarova, B. Sundqvist, R. Höhne, P. Esquinazi, Ya Kopelevich, P. Scharff, V.A. Davydov, L.S. Kashevarova, A.V. Rakhmanina, Magnetic carbon, Nature 413 (2001) 716–718, https://doi.org/10.1038/35099527.
[11] L.A. Chernozatonskii, V.A. Demin, P. Lambin, Bilayered graphene as a platform of nanostructures with folded edge holes, Phys. Chem. Chem. Phys. 18 (2016) 27432–27441, https://doi.org/10.1039/c6cp05082d.
[12] L.A. Chernozatonskii, V.A. Demin, A.A. Artyukh, Bigraphene nanomeshes: structure, properties, and formation, JETP Lett. (Engl. Transl.) 99 (2014) 309–314, https://doi.org/10.1134/S0021364014050051.
[13] E. Kano, A. Hashimoto, M. Takeguchi, B21-O-02 in situ TEM observation of Cu-doped graphene, Microscopy 64 (2015), https://doi.org/10.1093/jmicro/dfv131 i40.1-i40.
[14] D.G. Kvashnin, A.G. Kvashnin, E. Kano, A. Hashimoto, M. Takeguchi, H. Naramoto, S. Sakai, P.B. Sorokin, Two-dimensional CuO inside the supportive bilayer graphene matrix, J. Phys. Chem. C 123 (2019) 17459–17465, https://doi.org/10.1021/acs.jpcc.9b05353.
[15] N.A. Nebogatikova, I.V. Antonova, S.V. Erohin, D.G. Kvashnin, A. Olejniczak, V.A. Volodin, A.V. Skuratov, A.V. Krasheninnikov, P.B. Sorokin, L.A. Chernozatonskii, Nanostructuring few-layer graphene films with swift heavy ions for electronic application: tuning of electronic and transport properties, Nanoscale 10 (2018) 14499, https://doi.org/10.1039/c8nr03062f.
[16] J. Oh, H. Yoo, J. Choi, J.Y. Kim, D.S. Lee, M.J. Kim, J.C. Lee, W.N. Kim, J.C. Grossman, J.H. Park, S.S. Lee, H. Kim, J.G. Son, Significantly reduced thermal conductivity and enhanced thermoelectric properties of single- and bi-layer graphene nanomeshes with sub-10 nm neck-width, Nano Energy 35 (2017) 26–35, https://doi.org/10.1016/J.NANOEN.2017.03.019.
[17] S.V. Erohin, L.A. Chernozatonskii, P.B. Sorokin, On the edge of bilayered graphene: unexpected atomic geometry and specific electronic properties, J. Phys. Chem. Lett. 11 (2020) 5871–5876, https://doi.org/10.1021/ACS.JPCLETT.0C01341.
[18] Y. Yang, C. Han, B. Jiang, J. Iocozzia, C. He, D. Shi, T. Jiang, Z. Lin, Graphene-based materials with tailored nanostructures for energy conversion and storage, Mater. Sci. Eng. R Rep. 102 (2016) 1–72, https://doi.org/10.1016/j.mser.2015.12.003.
[19] E. McCann, M. Koshino, The electronic properties of bilayer graphene, Rep. Prog. Phys. 76 (2013) 28, https://doi.org/10.1088/0034-4885/76/5/056503.
[20] B. Partoens, F.M. Peeters, From graphene to graphite: electronic structure around the K point, Phys. Rev. B Condens. Matter 74 (2006), 075404, https://doi.org/10.1103/PhysRevB.74.075404.
[21] Y. Cao, J.Y. Luo, V. Fatemi, S. Fang, J.D. Sanchez-Yamagishi, K. Watanabe, T. Taniguchi, E. Kaxiras, P. Jarillo-Herrero, Superlattice-induced insulating states and valley-protected orbits in twisted bilayer graphene, Phys. Rev. Lett. 117 (2016) 116804, https://doi.org/10.1103/PhysRevLett.117.116804.
[22] K. Kim, A. DaSilva, S. Huang, B. Fallahazad, S. Larentis, T. Taniguchi, K. Watanabe, B. J LeRoy, A. H MacDonald, E. Tutuc, Tunable moiré bands and strong correlations in small-twist-angle bilayer graphene, Proc. Natl. Acad. Sci. U.S.A. 114 (2017) 3364–3369, https://doi.org/10.1073/PNAS.1620140114.
[23] K. Kim, M. Yankowitz, B. Fallahazad, S. Kang, H.C.P. Movva, S. Huang, S. Larentis, C.M. Corbet, T. Taniguchi, K. Watanabe, S.K. Banerjee, B.J. LeRoy, E. Tutuc, van der Waals heterostructures with high accuracy rotational alignment, Nano Lett. 16 (2016) 1989–1995, https://doi.org/10.1021/ACS.NANOLETT.5B05263.
[24] Y. Cao, V. Fatemi, A. Demir, S. Fang, S.L. Tomarken, J.Y. Luo, J.D. Sanches-Yamagishi, K. Watanabe, T. Taniguchi, E. Kaxiras, R.C. Ashoori, P. Jarillo-Herrero, Correlated insulator behaviour at half-filling in magic-angle graphene superlattices, Nature 556 (2018) 80–84, https://doi.org/10.1038/NATURE26154.
[25] T.C. Siu, T.A. Su, Conductivity in porous 2D materials made crystal clear, ACS Cent. Sci. 6 (2020) 11–13, https://doi.org/10.1021/acscentsci.9b01250.
[26] J. Jang, H.J. Jung, S. Chong, D. Kim, J. Kim, S.O. Kim, I. Kim, 2D materials decorated with ultra-thin and porous graphene oxide for high stability and selective surface activity, Adv. Mater. 32 (2020) 2002723, https://doi.org/10.1002/adma.202002723.
[27] G. Kresse, J. Hafner, Ab initio molecular dynamics for liquid metals, Phys. Rev. B 47 (1993) 558–561, https://doi.org/10.1103/PhysRevB.47.558.
[28] G. Kresse, J. Hafner, Ab initio molecular-dynamics simulation of the liquid-metalamorphous- semiconductor transition in germanium, Phys. Rev. B 49 (1994) 14251–14269, https://doi.org/10.1103/PhysRevB.49.14251.
[29] G. Kresse, J. Furthmüller, Efficient iterative schemes for ab initio total-energy calculations using a plane-wave basis set, Phys. Rev. B Condens. Matter 54 (1996) 11169–11186, https://doi.org/10.1103/PhysRevB.54.11169.
[30] P. Hohenberg, W. Kohn, Inhomogeneous electron gas, Phys. Rev. 136 (1964) B864, https://doi.org/10.1103/PhysRev.136.B864.
[31] W. Kohn, L.J. Sham, Self-consistent equations including exchange and correlation effects, Phys. Rev. 140 (1965) A1133, https://doi.org/10.1103/PhysRev.140.A1133.
[32] P.E. Blöchl, Projector augmented-wave method, Phys. Rev. B 50 (1994) 17953–17979, https://doi.org/10.1103/PhysRevB.50.17953.
[33] G. Kresse, D. Joubert, From ultrasoft pseudopotentials to the projector augmented-wave method, Phys. Rev. B 59 (1999) 1758–1775, https://doi.org/10.1103/PhysRevB.59.1758.
[34] J.P. Perdew, K. Burke, M. Ernzerhof, Generalized gradient approximation made simple, Phys. Rev. Lett. 77 (1996) 3865–3868, https://doi.org/10.1103/PhysRevLett.77.3865.
[35] S. Grimme, Semiempirical GGA-type density functional constructed with a long-range dispersion correction, J. Comput. Chem. 27 (2006) 1787–1799, https://doi.org/10.1002/jcc.20495.
[36] A.D. Becke, Density-functional exchange-energy approximation with correct asymptotic behavior, Phys. Rev. 38 (1988) 3098–3100, https://doi.org/10.1103/PhysRevA.38.3098.
[37] C. Lee, W. Yang, R.G. Parr, Development of the Colle-Salvetti correlation-energy formula into a functional of the electron density, Phys. Rev. B 37 (1988) 785–789, https://doi.org/10.1103/PhysRevB.37.785.
[38] V. Barone, Inclusion of Hartree-Fock exchange in the density functional approach. Benchmark computations for diatomic molecules containing H, B, C, N, O, and F atoms, Chem. Phys. Lett. 226 (1994) 392–398, https://doi.org/

10.1016/0009-2614(94)00725-X.
[39] V.A. Rassolov, M.A. Ratner, J.A. Pople, P.C. Redfern, L.A. Curtiss, 6-31G* basis set for third-row atoms, J. Comput. Chem. 22 (2001) 976–984, https://doi.org/10.1002/jcc.1058.
[40] P.C. Hariharan, J.A. Pople, The influence of polarization functions on molecular orbital hydrogenation energies, Theor. Chim. Acta 28 (1973) 213–222, https://doi.org/10.1007/BF00533485.
[41] U. Ruschewitz, R. Pöttgen, Structural phase transition in Li2C2, Z. Anorg. Allg. Chem. 625 (1999) 1599–1603, https://doi.org/10.1002/(SICI)1521-3749(199910)625:10<1599:AID-ZAAC1599>3.0.CO;2-J.
[42] Wigner, Zeitschrift fuer Physikalische Chemie, Abteilung B Chemie Der Elem. Aufbau Der Mater. 27 (1934) 37–49.
[43] The structure of crystals, in: second ed., in: R.W.G. Wyckoff (Ed.), American Chemical Society Monograph Series, vol. 37, Chemical Catalog Co., New York, 1931, p. 497, https://doi.org/10.1002/jctb.5000504413, 50, J. Soc. Chem. Ind. 50 (1931) 877–877.
[44] H.J. Zhang, J. Geng, C. Cai, Z.F. Ma, Z. Ma, W. Yao, J. Yang, Effect of doping order on metal-free heteroatoms dual-doped carbon as oxygen reduction electrocatalyst, Chin. Chem. Lett. (2020), https://doi.org/10.1016/j.cclet.2020.05.002.
[45] T.G. Tenev, N. V Vitanov, Can Electrostatic Field Lift Spin Degeneracy?, 2014 arXiv:1304.7968v2 [quant-ph].
[46] P. Carra, B.T. Thole, M. Altarelli, X. Wang, X-ray circular dichroism and local magnetic fields, Phys. Rev. Lett. 70 (1993) 694–697, https://doi.org/10.1103/PhysRevLett.70.694.
[47] A. Thompson, I. Lindau, D. Attwood, Y. Liu, E. Gullikson, P. Pianetta, M. Howells, A. Robinson, K.-J. Kim, J. Scofield, J. Kirz, J. Underwood, J. Korteight, G. Williams, H. Winick, X-Ray Data Booklet, third ed., Lawrence Berkeley National Laboratory, University of California, Berkeley, CA 94720, 2009.
[48] NIST X-ray Photoelectron Spectroscopy Database, in: NIST Standard Reference Database Number 20, National Institute of Standards and Technology, Gaithersburg MD, 2000, p. 20899, https://doi.org/10.18434/T4T88K. https://srdata.nist.gov/xps/ElmSpectralSrch.aspx?selEnergy=PE.
[49] K. Yamaguchi, F. Jensen, A. Dorigo, K.N. Houk, A spin correction procedure for unrestricted Hartree-Fock and M ller-Plesset wave functions for singlet diradicals and polyradicals, Chem. Phys. Lett. 149 (1988) 537–542, https://doi.org/10.1016/0009-2614(88)80378-6.
[50] K. Yamaguchi, H. Fukui, T. Fueno, Molecular-orbital (MO) theory for magnetically interacting organic compounds. ab-initio MO calculations of the effective exchange integrals for cyclophane-type carbene dimers, Chem. Lett. 15 (1986) 625–628, https://doi.org/10.1246/cl.1986.625.
[51] K. Tada, T. Maruyama, H. Koga, M. Okumura, S. Tanaka, Extent of spin contamination errors in DFT/plane-wave calculation of surfaces: a case of Au atom aggregation on a MgO surface, Molecules 24 (2019) 505, https://doi.org/10.3390/molecules24030505.
[52] K. Tada, S. Yamanaka, T. Kawakami, Y. Kitagawa, M. Okumura, K. Yamaguchi, S. Tanaka, Estimation of spin contamination errors in DFT/plane-wave calculations of solid materials using approximate spin projection scheme, Chem. Phys. Lett. 765 (2021) 138291, https://doi.org/10.1016/j.cplett.2020.138291.
[53] Y. Nagaoka, Ferromagnetism in a narrow, almost half-filled s band, Phys. Rev. 147 (1966) 392–405, https://doi.org/10.1103/PhysRev.147.392.
[54] E.A. Kovaleva, I. Melchakova, N.S. Mikhaleva, F.N. Tomilin, S.G. Ovchinnikov, W. Baek, V.A. Pomogaev, P. Avramov, A.A. Kuzubov, The role of strong electron correlations in determination of band structure and charge distribution of transition metal dihalide monolayers, J. Phys. Chem. Solid. 134 (2019) 324–332, https://doi.org/10.1016/j.jpcs.2019.05.036.